Improved ADRC-Based Integral Flux Observer for IPMSM Sensorless Control

Sadiq Ur Rahman[1*], Mahmood Ul Hassan [2], Yasir Iqbal [3], Muhammad Fahad [4]
[1] School of Electrical and Information Engineering, Tianjin University, Tianjin, China
[2] Foshan Noah Electrical Co., Ltd, Chancheng, Foshan, Guangdong, China.

Key Focus:
Offset → Error Reduction
Flux Stability

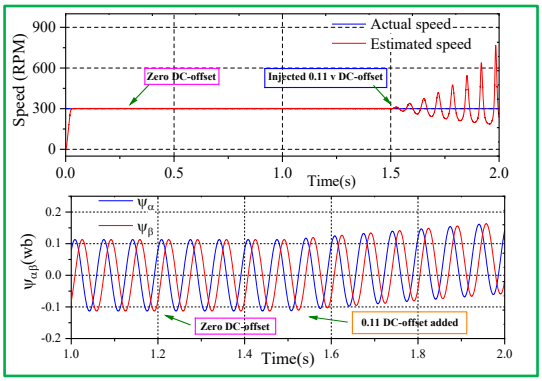

Proposed Flux Observer
Goal: Eliminate DC Offset
Result: Accurate Flux Estimate

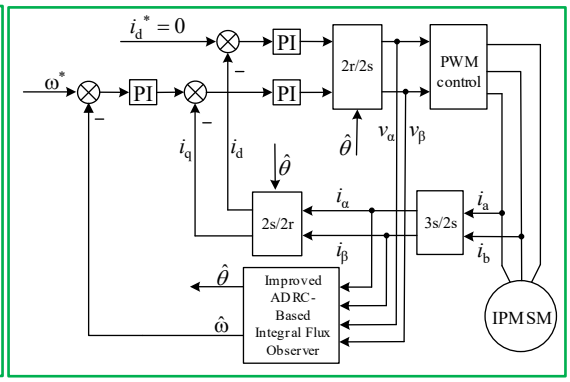

ABSTRACT: An interior Permanent magnet synchronous motor (IPMSM) drive employing sensorless control strategies offers to simplify the design of servo systems, reduce costs, and improve reliability, thus attracting significant research attention from both academic and industrial sectors for decades. The straightforward configuration and decreased application prerequisites make model-based sensorless control approaches highly popular. Notably, the conventional first-order integrator flux observer technique exhibits remarkable robustness owing to its minimal reliance on motor parameters. However, the conventional first-order integrator experiences a DC drift and harmonics in the estimated rotor flux as a result of non-ideal factors, such as detection errors, integral initial value, converter nonlinearities, and parameter mismatches. In this paper, an improved ADRC-based integral flux observer capable of eliminating drift is developed to achieve high-accuracy flux estimation. The efficiency of the proposed technique in eliminating the drift from the estimated flux, as evidenced by theoretical analysis, has no detrimental effect on the amplitude or phase angle of the fundamental waveform. The validity of the proposed improved ADRC-based integral flux observer is verified by sensorless vector control of a 7.5 [kW] three-phase IPMSM motor via extensive numerical simulation.

Keywords: Active Disturbance Rejection Control (ADRC); DC drift; Phase shift; conventional first-order integrator flux observer.

مراقب تدفُّق تكاملي مُحسَّن يعتمد على منهجية التحكم النشط في رفض الاضطرابات للتحكم الخالي من الحساسات في المحرك المتزامن ذو المغناطيس الدائم الداخلي

صديق الرحمن*، محمود الحسن، ياسر اقبال، محمد فهد

الملخص: يُعدّ استخدام محرك تزامني مغناطيسي دائم داخلي (IPMSM) مع استراتيجيات تحكم خالية من المستشعرات خيارًا مبتكرًا لتبسيط تصميم أنظمة السيرفو، وخفض التكاليف، وتعزيز الموثوقية. وقد حظي هذا المجال باهتمام واسع من الأوساط الأكاديمية والصناعية على مدى عقود. يتميز هذا النوع من المحركات بتصميم بسيط ومتطلبات تشغيل منخفضة، مما يجعل أساليب التحكم الخالية من المستشعرات المعتمدة على النماذج خيارًا شائعًا وفعالًا. تُظهر تقنية مراقبة التدفق باستخدام المُكامل التقليدي من الدرجة الأولى كفاءة عالية بسبب اعتمادها المحدود على معلمات المحرك. ومع ذلك، تواجه هذه التقنية تحديات تتمثل في حدوث انحراف مستمر (DC drift) واضطرابات في التدفق الدوار المُقدر نتيجة عوامل غير مثالية، مثل أخطاء القياس، والقيم الأولية للتكامل، وعدم خطية المحولات، وعدم توافق المعلمات .لمعالجة هذه التحديات، تقدم هذه الدراسة مراقب تدفق تكاملي محسّن يعتمد على تقنية التحكم النسبي المتقدم (ADRC) ، حيث تم تطويره لإزالة الانحراف وتحقيق تقدير دقيق للتدفق. أظهرت التحليلات النظرية كفاءة التقنية المقترحة في التخلص من الانحراف دون التأثير على سعة الموجة الأساسية أو زاوية طورها. وتم اختبار فعالية هذا النظام من خلال التحكم الاتجاهي الخالي من المستشعرات في محرك تزامني ثلاثي الأطوار بقدرة 7.5 كيلوواط، باستخدام محاكاة رقمية دقيقة تؤكد جدوى الحل المقدم.

الكلمات المفتاحية: التحكم في رفض الاضطرابات النشطة انحراف التيار المستمر; انزياح الطور; مراقب التدفق التقليدي بتكامل من الرتبة الأولى.

Corresponding author's e-mail: sadiqkhahak@tju.edu.cn

DOI:10.53540/tjer.vol.20iss2pp163-172

1. INTRODUCTION

An IPMSM is widely used across various industrial sectors due to its exceptionally high torque density and superior efficiency. To enhance efficacy in IPMSM speed drive systems, traditionally, a high-resolution mechanical sensor, such as a pulse encoder, is employed on the rotor shaft to accurately determine the rotor's position. However, integrating mechanical sensors increases costs and reduces reliability in speed drive systems. Therefore, in many applications, sensorless control is often necessary for IPMSMs to improve reliability, eliminate sensor wiring, reduce the motor's size and expenses, and achieve other related objectives (Wang et al., 2023; Woldegiorgis et al., 2023; Xiao et al., 2021).

In recent decades, numerous back EMF observers have been developed and utilized in commercial applications. Nevertheless, the back EMF signal deteriorates at low motor speeds, rendering these approaches ineffective in the low-speed range (Feng, Lai, & Mukherjee, 2017). Conversely, the flux estimator, which essentially integrates back EMF, can adeptly circumvent this issue due to its speed-independent amplitude. Despite this, a simple integrator is affected by drift problems since sensors consistently have a DC offset (DC_{off} (Xu et al., 2019; Liu et al., 2018; Jiang et al., 2019). One common approach is to replace the pure integrator with a low-pass filter, which can minimize the DC offset from the flux linkage observer. However, the low-pass filter has its limitations. When the motor speed is close to or below the filter's cutoff frequency, the effectiveness of the low-pass filter significantly diminishes, leading to inaccurate flux estimation and reduced performance in sensorless control systems (Kim et al., 2020; Li, Yang, & Wu, 2013).

Moreover, a flux observer based on SOIFO-FLL is suggested in (Kim et al., 2020; Li, Yang, & Wu, 2013), but it magnifies the challenges concerning harmonics and DC_{off}. Theoretical analysis indicates that its capability to eliminate DC is limited. A novel idea is introduced by Xu, Wang, Liu, and Blaabjerg (2019) for a third-order generalized integrator flux observer to enhance the capability of eliminating flux drift and reducing high-order harmonics in the estimated flux. Nonetheless, this approach is relatively complex to implement. A frequency-adaptive observer is suggested by Marchesoni, Passalacqua, Vaccaro, Calvini, and Venturini (2020). Both techniques can be considered adaptive high-order filters, relying on speed estimation, which negatively impacts performance. Wei Xu et al. (2019) proposed an enhanced rotor flux observer that incorporates a self-adaptive band-pass filter (SABPF) to attenuate high-frequency components and drift from the estimated rotor flux linkage. However, the inclusion of SABPF results in angle shifts that necessitate the adaptation of rotor speed for precise flux angle estimation. This process of speed calculation, typically the final stage, is susceptible to cumulative errors, noise, and time delays, which can lead to inaccuracies in the feedback loop and potentially compromise the accuracy of the speed and flux estimator over time.

Sadiq Ur Rahman et al. (2023) proposed two different DC_{off} compensators: a PI correction method and an ADRC-based DC_{off} compensator, both designed for sensorless PMSM motor drives equipped with wide-speed range flux linkage observers. Both feedback compensators effectively remove the DC_{off} from the system. However, both depend heavily on the accuracy of the current flux linkage observer's estimation of the rotor angle position.

In recent years, many new control strategies such as Active Disturbance Rejection Control (ADRC), Extended State Observer (ESO) and Nonlinear Extended State Observer (NESO) have achieved far beyond all existing linear optimal controllers. For instance, Han, Gao, and Dai (2009) presented a more robust ADRC method to improve fault tolerance against external disturbances. Additionally, Gao et al. Then, Tang et al. (2024) proposed a more feasible approach to ESOs while taking system uncertainties into account by giving conservative estimates. Zhang and his group (2011) have also shown that NESO outperforms existing nonlinear control techniques by large margins, in particular for high-order dynamics modelling and disturbance level-varied robustness.

In the domain of flux linkage observers, the ADRC feedback loop offers several advantages over conventional proportional-integral (PI) compensation loops. ADRC can handle a wider range of system dynamics and external disturbances without requiring accurate mathematical models, making the control algorithm more robust, adaptive, and fault-tolerant compared to standard PID controllers. GAO (2003) indicated that ADRC effectively coordinates system uncertainties and external disturbances, achieving more accurate force flux estimation compared to PI controllers. This technique is particularly beneficial for the sensorless control of Interior Permanent Magnet Synchronous Motors (IPMSMs), where model variations and environmental perturbations are prevalent.

In this paper, an improved integrator is applied to first-order ADRC to compensate for DC drifts in flux estimation during the sensorless control of IPMSMs. The study verifies, both numerically and theoretically, that this method significantly reduces drift by incorporating a first-order ADRC feedback loop. The proposed method demonstrates advantages over standard rotor flux estimators, particularly in saturation regions and under disturbances where commonly used methods fail to perform effectively. Consequently, the precision of calculated flux, speed, and rotor position is greatly enhanced. The efficacy of the suggested flux observer is validated through numerical simulation results. This work builds upon recent advancements in ADRC, ESO, and NESO, incorporating their strengths while

addressing their limitations in practical applications to IPMSMs.

2. ROTOR FLUX ESTIMATION PROBLEM

In the α-β stationary coordinate frame, the estimation of stator flux involves integrating the back EMF signal (e_{ss}) given by a mathematical expression (Xu et al., 2019):

$$\psi_{ss} = \int_0^t \left(u_{ss} - r_{sc} i_{ss}\right) = \int_0^t e_{ss} \tag{1}$$

where u_{ss} are stator voltage, r_{sc} stator resistance, and i_{ss} stator current, e_{ss} back-EMF, and ψ_{ss} is estimated stator flux linkage?
The frequency response of the integrator of equation (1) in the Laplace domain is as follows:

$$\frac{\psi_{ss}(s)}{e_{ss}(s)} = \frac{1}{s} \tag{2}$$

where $\frac{1}{s}$ is the integral in the Laplace transform? The estimated rotor flux linkage in the α-β coordinate frame is given by:

$$\begin{aligned} \psi_{r\alpha} &= \left(\int_0^t \left(u_{s\alpha} - r_{sc} i_{s\alpha}\right)\right) - L_q i_{s\alpha} \\ \psi_{r\beta} &= \left(\int_0^t \left(u_{s\beta} - r_{sc} i_{s\beta}\right)\right) - L_q i_{s\beta} \end{aligned} \tag{3}$$

where $\psi_{r\alpha}, \psi_{r\beta}$ are the estimated rotor flux linkage in the α and β axes, respectively? $u_{s\alpha}, u_{s\beta}$ Are the stator voltages in the α and β axes, respectively? r_{sc} Represents the stator resistance. $i_{s\alpha}$ And $i_{s\beta}$ are the stator currents in the α and β axes, respectively. L_q Denotes the quadrature-axis inductance.

The rotor position angle, $\hat{\theta}_{est}$, can then be estimated using the arctangent function, which relates the α and β components of the rotor flux linkage:

$$\hat{\theta}_{est} = \arctan \frac{\psi_{r\beta}}{\psi_{r\alpha}} \tag{4}$$

The derivation of the stator flux linkage vector entails the integration of the EMF, as depicted in equation (1). However, two primary challenges arise: firstly, any offsets in voltage or current measurements result in substantial drifts in the calculated stator flux linkage, and secondly, initializing the simple integrator with an incorrect value (e.g., Initial rotor phase) introduces a DC_{off} at the output of the integrator. The presence of a DC component within a loop can introduce oscillation. The bode plot illustrating the characteristics of a pure integrator is depicted in Figure 1.

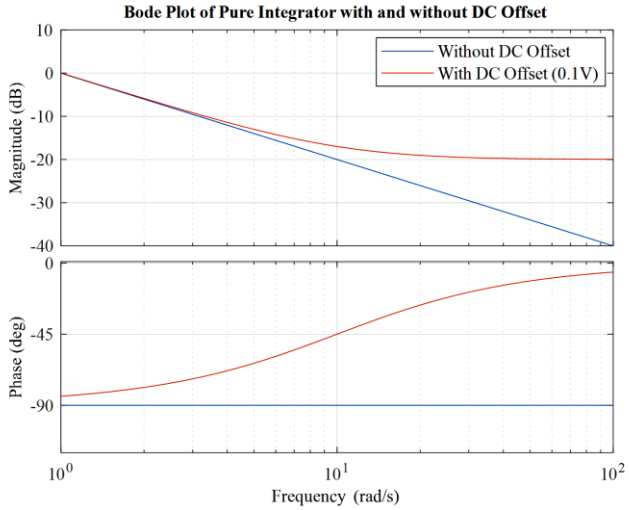

Figure 1. Bode plot of pure integrator.

As per Figure 1, the existence of DC_{off} disrupts the phase response of the pure integrator, leading to inaccuracies in signal integration, especially at lower frequencies. This departure from the desired -90-degree phase response indicates a decline in the performance of the integrator, ultimately affecting its capability to eradicate steady-state error and uphold stability in control systems efficiently. To address these problems, a frequently employed approach involves substituting the pure integrator with a first-order low-pass (LP) filter. The calculated stator flux by the LP filter can be stated as:

$$\frac{\psi_{ss}(s)}{e_{ss}(s)} = \frac{1}{s+a} \tag{5}$$

Where a is a pole. The phase shift and the gain of (5) is given as:

$$\varphi = -\tan^{-1}\left\{\frac{\omega_{est}}{a}\right\} \tag{6}$$

$$A = \left|\left(\frac{\psi_{sp}}{e_{ss}}\right)\right| = \frac{1}{\sqrt{\omega_{est}^2 + a^2}} \tag{7}$$

where ω_{est} is an estimated synchronous angular frequency? Figure 2 displays the phase lag ψ_{sp} as determined by the LPF, as well as the phase lag ψ_{ss} as calculated by the integrator. The phase delay ψ_{ss} equates to $\frac{\pi}{2}$, with a gain of $\frac{1}{\omega_{est}}$. However, it should be noted that the phase delay of the LP filter is not $\frac{\pi}{2}$, nor is the gain $\frac{1}{\omega_{est}}$. As a result of this discrepancy, an error will arise due to the impact of the LP filter. This error becomes

more pronounced when the IPMSM frequency falls below the corner frequency of the LP filter. The LP filter in (4) must possess an extremely low cutting frequency to rectify this error. Nevertheless, the drift issue persists due to the LP filter's substantial time constant. In order to achieve an accurate estimation of the stator flux, it is imperative that the phase delay and gain of ψ_{sp} in (5) are set at $\frac{\pi}{2}$ and $\frac{1}{\omega_{est}}$, respectively.

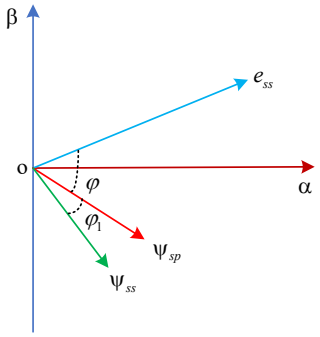

Figure. 2. Vector diagram of pure integrator and LP filter.

The Self-Adaptive Band-Pass Filter (SABPF) is designed to remove the DC component and high-frequency harmonics from the estimated rotor flux linkage. The SABPF is designed using the following transfer function [9]:

$$G(s)=\frac{\hat{v}}{v}=\frac{q\omega_r s}{s^2+q\omega_r s+\omega_r^2} \tag{8}$$

where v is the input of the SABPF, $\hat{v}$ is the output of the SABPF, q is the quality factor, and ω_r is the self-adaptive resonance angular frequency? The amplitude-frequency characteristic of the SABPF is given by:

$$G(\omega)=\frac{q\omega_r\omega}{\sqrt{\left(\omega^2-\omega^2{}_r\right)^2+\left(q\omega_r\omega\right)^2}} \tag{9}$$

where ω is the rotor angular speed? The phase-frequency characteristic of the SABPF is:

$$\angle G(\omega)=\tan^{-1}\left(\frac{\omega^2{}_r-\omega^2}{q\omega_r\omega}\right) \tag{10}$$

The SABPF is applied to the output of the conventional flux observer:

$$\begin{aligned}\hat{\psi}_{r\alpha}&=G(s).\psi_{r\alpha}=\frac{q\omega_r s}{s^2+q\omega_r s+\omega_r^2}\psi_{r\alpha}\\ \hat{\psi}_{r\beta}&=G(s).\psi_{r\beta}=\frac{q\omega_r s}{s^2+q\omega_r s+\omega_r^2}\psi_{r\beta}\end{aligned} \tag{11}$$

The quality factor q determines the bandwidth and selectivity of the filter. The bandwidth of the filter is inversely proportional to the quality factor:

$$\begin{aligned}\Delta\omega&=\frac{\omega_r}{q}\\ Q&=\frac{\omega_r}{\Delta\omega}=q\end{aligned} \tag{12}$$

A higher q factor in a SABPF filter results in a narrower bandwidth, enhancing selectivity and better rejecting unwanted frequencies. Conversely, a lower q factor broadens the bandwidth, reducing selectivity and allowing more frequencies to pass. The filter's selectivity is defined by its ability to sharply distinguish between desired and undesired frequencies. This is often measured by the filter's Q-factor. Higher Q means higher selectivity.

The SABPF filter's ability to attenuate unwanted frequencies is also influenced by q. The SABPF filter's gain at a given frequency ω is:

$$\left|G(j\omega)\right|=\frac{q\omega_r\omega}{\sqrt{\left(\omega^2-\omega^2{}_r\right)^2+\left(q\omega_r\omega\right)^2}} \tag{13}$$

For effective attenuation of unwanted frequencies, q should be chosen such that the response is minimized at those frequencies. Variations in ω_r or q can lead to deviations in the filter's frequency response, affecting its ability to accurately filter the desired signal components. From Equation (10), the phase shift may be generated due to the mismatch of self-adaptive resonant angular frequency and estimated rotor angular frequency. Therefore, the phase shift can be compensated by Equation (14), obtain the estimated rotor position as follows:

$$\hat{\theta}=\tilde{\hat{\theta}}-\tan^{-1}\left(\frac{\omega^2{}_r-\omega^2}{q\omega_r\omega}\right) \tag{14}$$

The performance of the SABPF is highly sensitive to the accurate tuning of the resonance angular frequency Variations ω_r and the quality factor q. A slight mismatch can result in significant errors and the estimated rotor position $\hat{\theta}$ will be incorrect, leading to rotor position and speed errors.

In this work, to address this issue, a specialized Active Disturbance Rejection Control (ADRC) feedback approach will be incorporated to counterbalance the DC_{off} and establish stability in the estimation of the stator flux.

The transfer function of the disturbance and controller observer of ADRC is given by:

$$G_D(s) = \frac{\omega_0}{s+\omega_0}$$
$$G_c(s) = \frac{\omega_c s+1}{s+\omega_c} \quad (15)$$

where, ω_0 , ω_c are a disturbance and controller observer. The composite transfer function of the feedback ADRC system, derived from the product of the controller and disturbance observer transfer functions, is presented as follows:

$$G_{adrc}(s) = \frac{\omega_0}{s+\omega_0}.\frac{\omega_c s+1}{s+\omega_c} \quad (16)$$

The closed-loop transfer function with ADRC is obtained by connecting the ADRC system in feedback with the transfer function of the pure integrator with the DC_{off}. Mathematically, it's represented as:

$$G(s) = \frac{G_{adrc}(s).G_{\text{int}}(s)}{1+G_{adrc}(s).G_{\text{int}}(s)} \quad (17)$$

where $G_{\text{int}}(s)$ is the transfer function of the integrator with the DC_{off}? In the absence of ADRC, system stability is contingent solely upon the dynamics of the integrator with the DC_{off}. The presence of DC_{off} can potentially introduce additional poles in the right-half plane, thereby impacting system stability. The ADRC methodology introduces supplementary dynamics through its controller and disturbance observer. By integrating feedback from the disturbance observer, ADRC aims to alleviate the disruptive effects of disturbances, including DC_{off}, on system performance. Operating in real-time, the ADRC system dynamically adjusts system response to effectively mitigate disturbances, consequently enhancing both stability and overall performance.

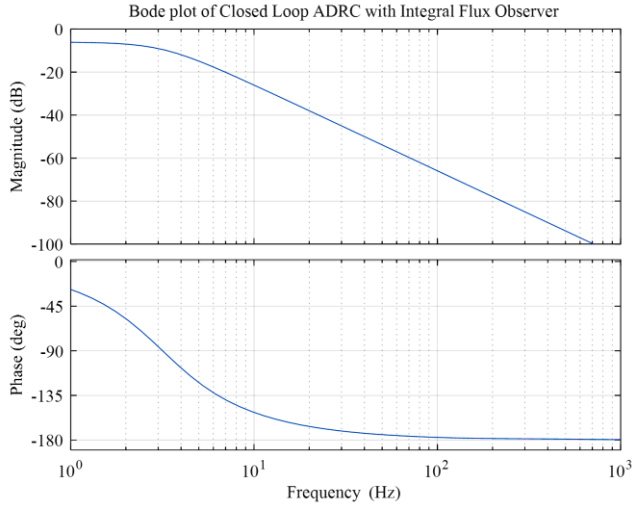

Figure 3. Bode plot of Integral flux observer with ADRC feedback loop.

As per Figure 3, the phase plot elucidates the system's phase shift characteristics across varying frequencies. At lower frequency ranges, the phase tends asymptotically towards zero degrees, indicative of minimal phase deviation. As frequency escalates, the phase shift progressively trends towards more negative values, culminating at -180 degrees for stable systems operating at high frequencies. Notably, at 1000 Hz, the phase plot attains a phase shift of precisely -180 degrees, mirroring the behaviour of a pure integrator. Concurrently, the magnitude plot registers a descent to -100 dB at this frequency, reflecting pronounced attenuation in the input signal.

A first-order ADRC centred on an Extended State Observer (ESO) and a feedback control law. The observer is designed to estimate the system state, the stator flux, and the combined disturbance, i.e., the DC_{off}. The ESO is mathematically represented as follows:

$$\dot{\hat{z}}_1 = \hat{z}_2 + L_1\left(y-\hat{z}_1\right)$$
$$\dot{\hat{z}}_2 = L_2\left(y-\hat{z}_1\right) \quad (18)$$

where $\hat{z}_1$ represents the estimated stator flux, $\hat{z}_2$ includes the overall estimated disturbance, and y or corresponds to the measured stator flux. The observer's gains L_1 and L_2 are carefully adjusted in order to comply with an observer bandwidth, guaranteeing a timely and precise measurement of the flux and disturbances. The feedback control mechanism of the ADRC utilizes the estimation of disturbances to produce a control action (u_{cmp}) that effectively nullifies the direct current offset, thus enhancing the estimation of stator flux. The control law can be concisely stated as follows:

$$u_{cmp} = -\frac{1}{\hat{b}}\left(\hat{z}_2\right) \quad (19)$$

where $\hat{b}$, is the input gain, preset to unity. This control input is then used to adjust the back electromotive force (EMF), directly impacting the stator flux estimation by removing the unwanted DC_{off}. By incorporating this control measure into the voltage model of the IPMSM within the feedback loop, to calculate the adjusted rotor flux ($\psi_{r\alpha}, \psi_{r\beta}$):

$$\psi_{r\alpha} = \left(\int_0^t \left(u_{s\alpha} - r_{sc} i_{s\alpha}\right) - \left(u_{cmp}\right)\right) - L_q i_{s\alpha}$$
$$\psi_{r\beta} = \left(\int_0^t \left(u_{s\beta} - r_{sc} i_{s\beta}\right) - \left(u_{cmp}\right)\right) - L_q i_{s\beta} \quad (20)$$

Utilizing the feedback ADRC-based strategy has significantly enhanced the drift issue. It has resulted in accurately estimating the stator flux across a wide range of speeds. In a traditional flux observer, the rotor position can solely be acquired through equation (4). However, motor control also necessitates knowledge of the rotor

speed. When differentiation is applied to generate the rotor speed, it may produce high-order harmonics in the projected rotor speed. Consequently, PLL is employed to acquire both the projected rotor position and speed. The schematic overview of the feedback ADRC and integral flux observer with PLL is depicted in Figure 4.

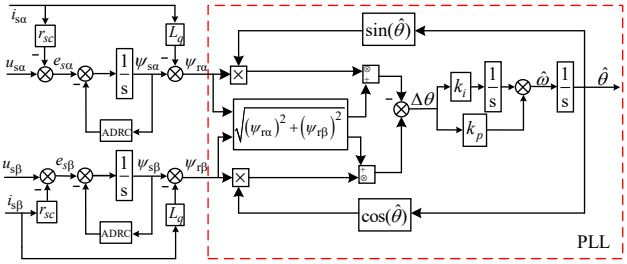

Figure. 4. Structure diagram of enhanced flux observer with ADRC for DC_{off} compensation loop.

3. SIMULATION RESULTS

The diagram shown in Figure 5 illustrates the sensorless control system based on the proposed method. The foundational control method used is the FOC scheme. Initially, the sampled voltage and current undergo αβ transformation to derive the αβ axis current and voltage components. Subsequently, the calculated angular speed and motor rotor position are determined utilizing the proposed methodology. Concurrently, the calculated angular speed is integrated into the angular speed loop, while the estimated motor rotor position facilitates the execution of dq transformation and inverse Park transform operations. Additionally, Table 1 enumerates the parameters pertinent to the tested motor.

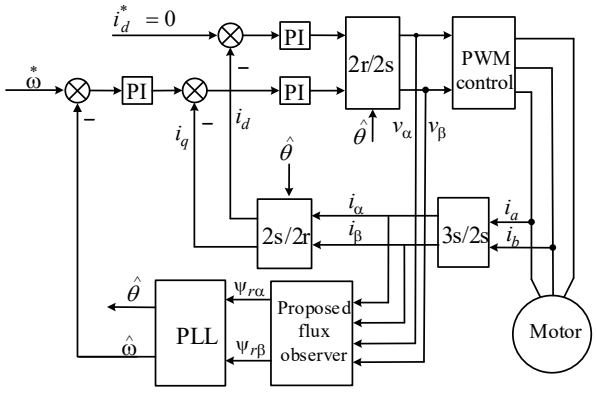

Figure 5. Diagram illustrating sensorless control strategy utilizing proposed flux observer.

Table 1. Parameters of IPMSM and ADRC-controller.

Parameter	Value
Nominal speed	3.0e3 RPM
STATOR D-AXIS INDUCTANCE	0.000348H
Stator phase resistance	0.1 Ω
Pole pairs	3
Stator q-axis inductance	0.000558 H
Rated power	7500 W
ADRC observer bandwidth	20 rad/s
ADRC controller bandwidth	10 rad/s

3.1 Simulated Data Analysis

Figure 6 presents the simulation outcomes with respect to the calculated stator flux linkage utilizing a traditional flux observer at a speed of 700 r/min in the absence of any load.

Figure 6 (a) illustrates that without any DC_{off}, the conventional flux observer effectively estimates the stator flux with no observable drift phenomenon. However, in Figure 6(b), when a 0.1 V DC_{off} is injected into the stator voltage on the alpha-axis, as is common in practical scenarios due to the presence of a DC_{off} in the measured motor back EMF, the pure integrator can be driven into saturation, even with a small DC_{off}.

Figure 7 depicts the computer simulation results for the estimated speed and rotor position using a conventional flux observer at 700 (r/min) under no-load conditions. Figure 7(a) shows the injected DC_{off}, actual rotor speed, estimated rotor speed, and speed estimation error in RPM. Figure 7(b) displays the injected DC_{off}, actual angle, estimated angle, and angle estimation error in degrees. As observed from Figure 7, when there is no DC_{off}, the conventional flux observer effectively estimates rotor speed and position with a steady-state error around zero. However, when a DC_{off} is injected at 1.505 seconds, oscillations in the estimated speed and rotor angle are observed, which can ultimately drive the pure integrator into saturation.

Figure 8 depicts the simulation results for the estimated stator flux linkage using a proposed flux observer at 700 r/min under no-load conditions. Figure 8(a) illustrates that without any DC_{off}, the proposed flux observer effectively estimates the stator flux with no observable drift phenomenon. However, in Figure 8(b), some drift is observed when a 0.2 V DC_{off} is added to the stator voltage on the alpha-axis. Nevertheless, due to the ADRC feedback loop, the drift phenomenon is effectively eliminated.

Figure 9 illustrates simulation results for speed and rotor position estimation using an ADRC algorithm with DC_{off} compensation in the flux observer at 700 r/min under no-load conditions. Figure 9(a) shows injected DC_{off}, actual and estimated rotor speed, and speed estimation error in RPM. Figure 9(b) displays the injected DC_{off}, actual and estimated angle, and angle estimation error in degrees.

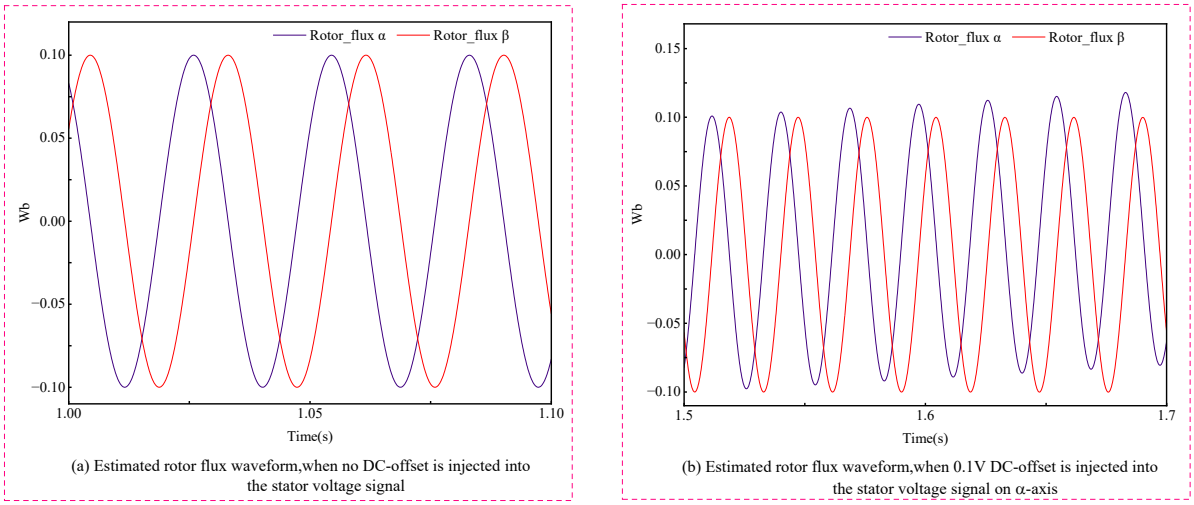

Figure 6. Simulation results of stator flux estimation with conventional flux observer at 700 r/min under no-load conditions.

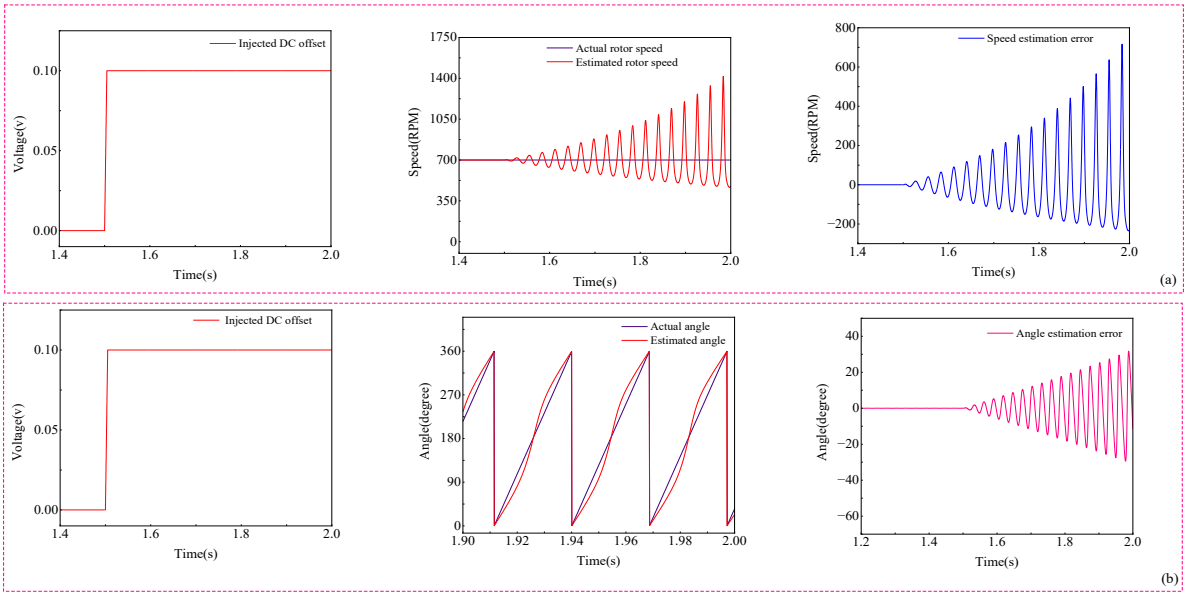

Figure 7. Simulation results of estimated speed and rotor position using conventional flux observer at 700 r/min without load condition.

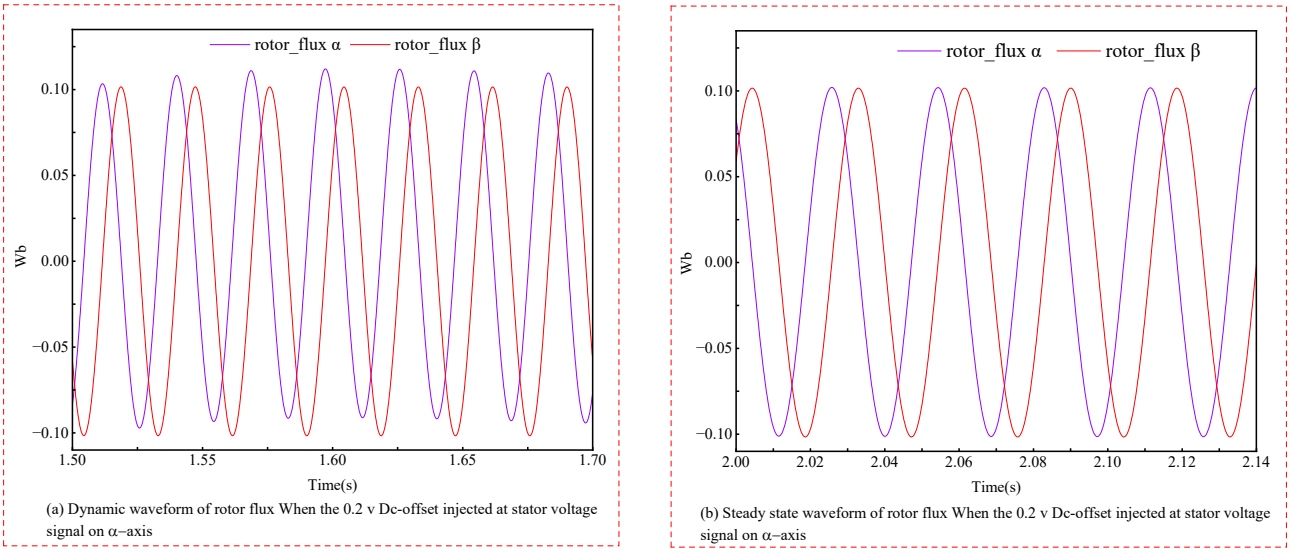

Figure 8. Simulation findings of stator flux estimation with the proposed observer at 700 r/min under no-load conditions.

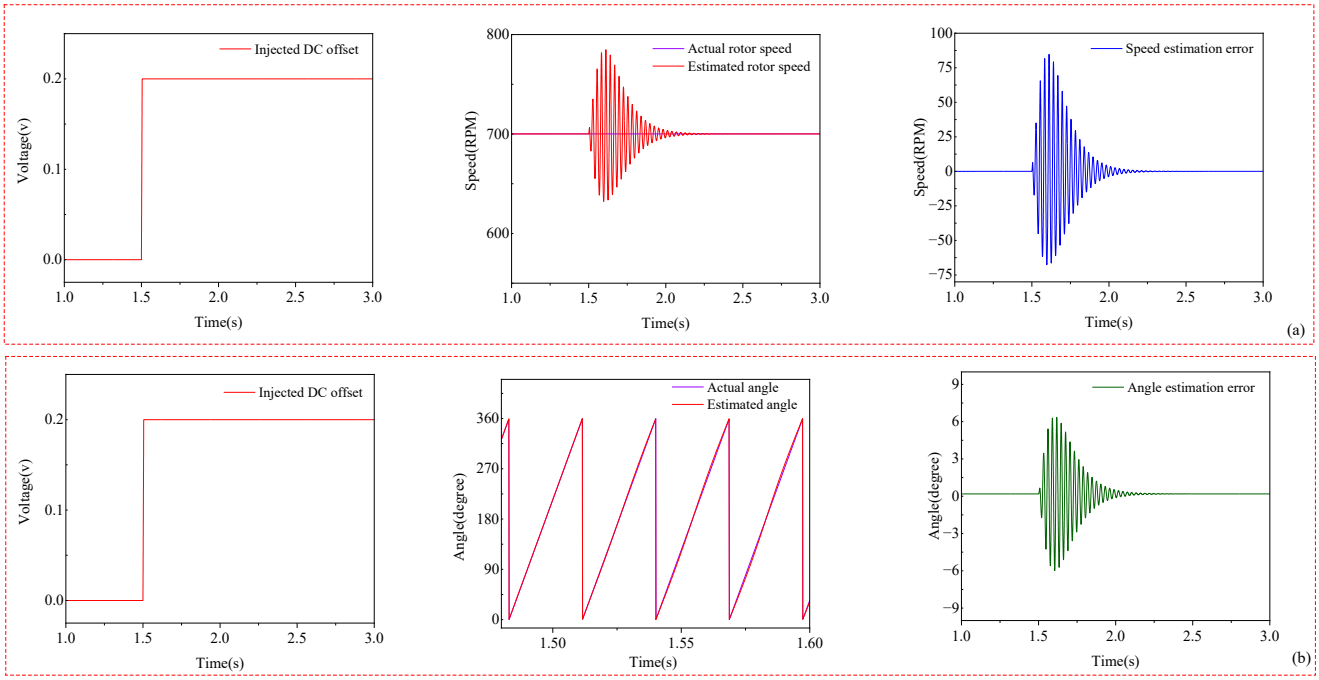

Figure 9. Simulation results of speed and rotor position estimation with First-Order ADRC and DC_{off} compensation.

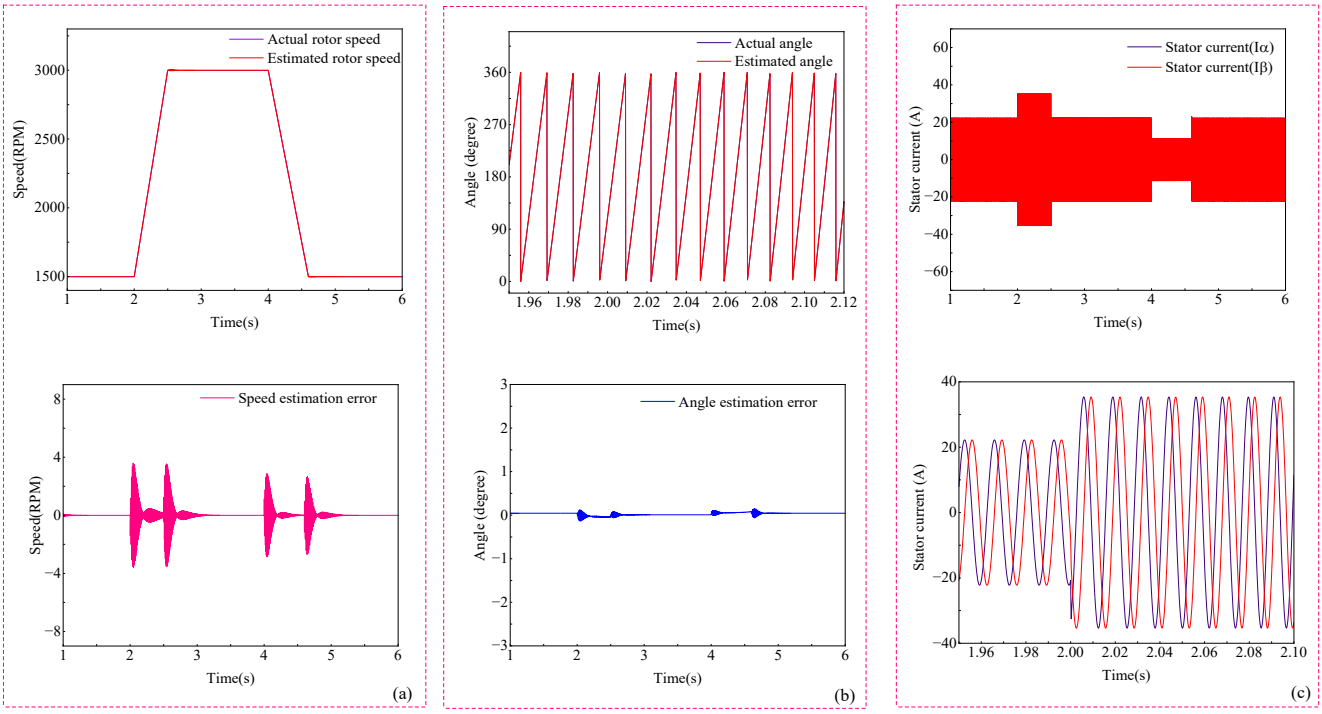

Figure. 10. Performance evaluation of proposed method with speed step change and constant load torque.

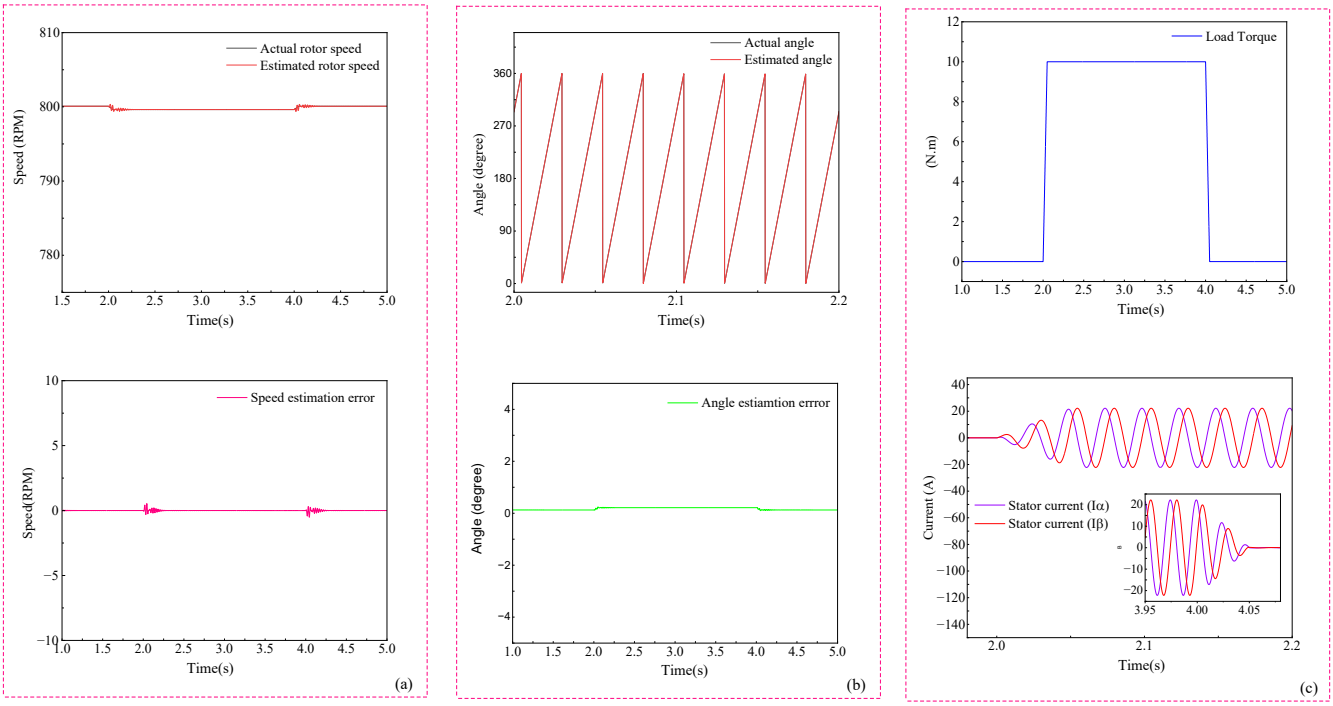

Figure. 11. Simulation results of the proposed method under sudden load changes.

In the absence of DC_{off}, the flux observer accurately estimates rotor speed and position with minimal steady-state error. However, with a 0.2 V DC_{off} injected at 1.505 seconds, estimated speed and rotor angle oscillations occur. The ADRC feedback loop effectively removes the DC_{off}, ensuring system stability. This approach estimates and mitigates unknown disturbances, such as the DC_{off} in stator flux.

A speed step change was implemented to verify its effectiveness with a constant load torque of 10 Nm. Initially, the IPMSM motor operated at 1500 rpm. At 2.05 seconds, the speed stepped to the rated speed of (3000 rpm), then reduced back to 1500 rpm at 4.8 seconds, as shown in Figure 10. Performance Evaluation of Proposed Method with Speed Step Change and Constant Load Torque.

Figure 10(a) depicts the actual speed, estimated speed, and speed estimation error in rpm. The speed estimation error did not exceed 5 rpm during speed transitions. Figure 10(b) presents the actual angle, estimated angle, and angle estimation error in degrees. Remarkably, the angle estimation error remained below 0.2 degrees. Figure 10(c) shows the motor stator currents in the alpha-beta waveform when the IPMSM speed stepped with constant load. Figure 10(c) illustrates that when the speed changes to 3000 rpm and reduces to 1500 rpm, the motor stator current is sinusoidal with no overshoot. Figure 11(a) presents the actual rotor speed, estimated rotor speed, and the estimation error between the actual and estimated speeds.

Figure 11(b) depicts the actual angle, estimated angle, and angle estimation error when the load is suddenly applied at 2 seconds. Figure 11(c) demonstrates the load torque waveform and the motor stator current in the alpha-beta frame when the load is suddenly applied and removed.

Figure 11(a) shows that when the load is applied, the estimation error does not exceed 2.5 rpm, and the steady-state error is close to zero, indicating that the proposed method effectively estimates the actual rotor speed. Figure 11(b) shows that the maximum error when the load is applied and removed does not exceed 0.5 degrees, further confirming the effectiveness of the proposed method. Figure 11(c) illustrates that when the load is suddenly applied and removed, the motor stator current is sinusoidal with no overshoot.

4. CONCLUSION

The paper presents a proposed integration algorithm with First Order ADRC to compensate the DC_{off} loop for estimating motor flux. The algorithm is thoroughly examined and compared. Its development is aimed at addressing practical issues associated with pure integrators for IPMSM flux estimation. Compared to the low-pass filter and the SABPF, the proposed method does not cause any angle shift. Therefore, there is no need for a compensation block, making this method simpler and more accurate. The simulation results demonstrate the proposed method's superior dynamic and steady-state performance. Its robust performance under varying conditions supports its suitability for dynamic motor control systems. The proposed algorithm is well-suited for high-performance sensorless IPMSM drivers that may encounter variations in motor flux during operation. Future research could focus on improving the accuracy of

the position estimation, primarily when the motor operates at low speeds or during startup conditions, where sensorless control methods typically face challenges. Another area for future work could be the implementation of the proposed method in real-world applications to test its robustness and reliability under various operating conditions, such as changes in load or the presence of electrical noise.

CONFILCT OF INTEREST

The authors declare that there are no conflicts of interest regarding this article.

FUNDING

The authors did not receive any funding for this research.

REFERENCES

Wang, J., Ma, J., Zhao, X., Meng, D., Xu, K., & Guo, D. (2023). Sensorless control strategy for interior permanent magnet synchronous motors in the full-speed section. *Energies, 16*(7701), 1-16.

Hu, J., & Wu, B. (1998). New integration algorithms for estimating motor flux over a wide speed range. *IEEE Transactions on Power Electronics, 13*(6), 969–977.

Xiao, D., Nalakath, S., Filho, S. R., Fang, G., Dong, A., Sun, Y., Wiseman, J., & Emadi, A. (2021). Universal full-speed sensorless control scheme for interior permanent magnet synchronous motors. *IEEE Transactions on Power Electronics, 36*(6), 4723–4737.

Feng, G., Lai, C., & Mukherjee, K. (2017). Online PMSM magnet flux estimation for rotor magnet condition monitoring using harmonics in speed measurements. *IEEE Transactions on Industry Applications, 53*(5), 2786–2794.

Xu, W., Jiang, Y., Mu, C., & Blaabjerg, F. (2019). Improved nonlinear flux observer-based second-order SOIFO for PMSM sensorless control. *IEEE Transactions on Power Electronics, 34*(2), 565–579.

Liu, K., Feng, J. H., Guo, S. Y., Xiao, L., & Zhu, Z. Q. (2018). Identification of flux linkage map of permanent magnet synchronous machines under uncertain circuit resistance and inverter nonlinearity. *IEEE Transactions on Industrial Informatics, 14*(2), 556–568.

Jiang, Y., Xu, W., Mu, C., Zhu, J., & Dian, R. (2019). An improved third-order generalized integrator flux observer for sensorless drive of PMSMs. *IEEE Transactions on Industrial Electronics, 66*(11), 9149–9160.

Kim, H.-S., Sul, S.-K., Yoo, H., & Oh, J. (2020). Distortion-minimizing flux observer for IPMSM based on frequency-adaptive observers. *IEEE Transactions on Power Electronics, 35*(3), 2077–2087.

Xu, W., Wang, L., Liu, Y., & Blaabjerg, F. (2019). Improved rotor flux observer for sensorless control of PMSM with adaptive harmonic elimination and phase compensation. *CES Transactions on Electrical Machines and Systems, 3*(2), 151–159.

Marchesoni, M., Passalacqua, M., Vaccaro, L., Calvini, M., & Venturini, M. (2020). Performance improvement in a sensorless surface-mounted PMSM drive based on rotor flux observer. *Control Engineering Practice, 96*, Article 104276.

Adelekan, D. S., Ohunakin, O. S., & Paul, B. S. (2022). Artificial intelligence models for refrigeration, air conditioning, and heat pump systems. *Energy Reports, 8*, 8451–8466.

Sadiq Ur Rahman, et al. (2023). DCoff compensators for sensorless PMSM motor drives equipped with wide speed range flux linkage observers. *Journal of Physics: Conference Series, 2591*, Article 012048.

Han, J., Gao, Z., & Dai, H. (2009). Active disturbance rejection control: A paradigm shift in feedback control system design. *IEEE Transactions on Industrial Electronics, 56*(3), 900–906.

Wang, G., Xue, W., Peng, H., Yang, Z., & Zhao, Y. (2024). Parallel multiple extended state observers based ADRC with application to high-speed precision motion stage. *IEEE Transactions on Industrial Electronics, 71*(8), 9639–9648.

Zhang, Y., & Sun, Q. (2011). Nonlinear extended state observer for multivariable nonlinear systems with coupled uncertainties. *Journal of Control Theory and Applications, 9*(4), 362–366.

Li, X., Yang, S., & Wu, Z. (2013). Limitations of low-pass filters in sensorless control of IPMSM. *IEEE Transactions on Industrial Electronics, 60*(9), 3800–3809.

Gao, Z. (2003). An active disturbance rejection control approach to tension and speed regulation in the coiling-uncoiling process. *Proceedings of the IEEE 30th Annual Conference of Industrial Electronics Society, 2*, 1551–1557.